JOURNAL OF Applied Polymer SCIENCE

Compressive mechanical properties of HTPB propellant at low, intermediate, and high strain rates

Long Yang,[1] Kan Xie,[1] Jiangfeng Pei,[2] Xin Sui,[1] Ningfei Wang[1]

[1]School of Aerospace Engineering, Beijing Institute of Technology, Beijing 100081, People's Republic of China

[2]Science and Technology on Combustion and Explosion Laboratory, Xi'an Modern Chemistry Research Institute, Xi'an, Shanxi 710065, People's Republic of China

Correspondence to: K. Xie (E-mail: xiekan1982@126.com)

ABSTRACT: Low, intermediate, and high strain rate compression testing (1.7×10^{-4} to 2500 s^{-1}) of the hydroxyl-terminated polybutadiene (HTPB) propellant at room temperature, were performed using a universal testing machine, a hydraulic testing machine, and a split Hopkinson pressure bar (SHPB), respectively. Results show that the stress linearly increases with strain at each condition; the increasing trend of stress at a given strain with the logarithm of strain rate changes from a linear to an exponential form at 1 s^{-1}. By combining these characteristics, we propose a rate-dependent constitutive model which is a linearly elastic component as a base model, then multiplied by a rate-dependent component. Comparison of model with experimental data shows that it can characterize the compressive mechanical properties of HTPB propellant at strain rates from 1.7×10^{-4} to 2500 s^{-1}. © 2016 Wiley Periodicals, Inc. J. Appl. Polym. Sci. **2016**, *133*, 43512.

KEYWORDS: composites; mechanical properties; properties and characterization

Received 11 October 2015; accepted 3 February 2016

DOI: 10.1002/app.43512

INTRODUCTION

HTPB propellant is a lightly cross-linked polymer filled with a certain amount of solid particles.[1] It has been extensively used in solid rocket motors (SRMs) for gun-launched missiles, because of its high energy density, and good process and mechanical properties. To achieve an initial speed of several hundred meters per second in a few milliseconds, the SRMs tend to support a high overload of up to 10^4 times the acceleration because of gravity. Such an overload is far higher than that of 10^1 times the acceleration because of gravity supported by the conventional missiles, which constitutes a great challenge for the structure integrity of solid propellant grain, and the security and reliability of SRMs. In high overload applications, solid propellant is subjected to impact loading under strain rates of the order of 10^2 s^{-1} (so-called intermediate strain rates). Because of a lack of dynamic experimental data, the quasi-static mechanical properties of solid propellant have been even used to evaluate the structure integrity of solid propellant grain. The evaluation method may cause a large error because of the significant differences between the quasi-static and dynamic mechanical properties[2] It is the goal of this work to study the mechanical properties of HTPB propellant at low, intermediate, and high strain rates, which facilitate the structural integrity analysis of solid propellant grain under high overload conditions.[3,4]

A thorough understanding of the rate-dependent mechanical properties of HTPB propellant is extremely important. However, there are relatively little related reports in the extant literature. A huge volume of literature exists on the rate-dependent mechanical properties of a variety of polymers. Chou *et al.*[5] examined the compressive behaviors of polymethyl methacrylate (PMMA), cellulose acetate butyrate (CAB), polypropylene (PP), and polyamide (PA) over a wide range of strain rates. In particular, he plotted the flow stress at a given strain level as a function of the logarithm of strain rate. It was found that the stress increased bilinearly with the logarithm of strain rate, with a higher slope at high strain rates. The bilinear strain-rate dependence was also observed by Siviour[6] for polycarbonate (PC) and polyvinylidene difluoride (PVDF), Mulliken[7] for PC and PMMA, Jordan[8] for epoxy, Yi[9] for polyurea and polyurethane (PU). Walley *et al.*[10] examined the compressive behaviors of a large number of polymers at room temperature over strain rates ranging from 10^{-2} to 10^4 s^{-1}. Again, they plotted the yield stress as a function of the logarithm of strain rate, and found that the materials tested fell into three different groups: a linear dependence, with a constant slope over a wide range of strain rates; a bilinear dependence, with a dramatic increase in slope at a strain rate of *c.* 10^3 s^{-1}; a decrease in maximum stress at a strain rate of *c.* 10^3 s^{-1}, possibly followed by an increase. Interpretation for these behaviors is mainly focused on the

Table I. Composition of HTPB Propellant

Component	Al	RDX	AP	HTPB	Other additives
Content (wt %)	5	20	60	9	6

bilinear strain-rate dependence. Previous researchers,[6–9] by combining the shifting data of transition location from dynamic mechanical analysis (DMA) curves, identified that the bilinearity of different materials is because of the movement of different transitions past room temperature. The transition is unique to the particular polymer.

The rate-dependent mechanical behaviors of polymers have been predicted by many models. Bergstrom and Boyce,[13,14] by combining two interacting macromolecular networks, proposed a model to describe the mechanical responses of elastomers over a wide range of strain rates. The two networks are represented by the Arruda-Boyce eight-chain model, and another eight-chain network with a relaxed configuration, respectively. However, it is very difficult to determine the parameters in the model by experiments. Yang *et al.*,[15,16] by combining hyperelastic and viscoelastic theories, proposed a visco-hyperelastic constitutive model to describe the large deformation response of rubber at high strain rates. Although Pouriayevali[17] and Khajehsaeid[18] modified the relaxation time, the model cannot still describe the mechanical behavior over a wide range of strain rates. Based on Yang's work, Zhang *et al.*[19] used two viscoelasticity elements instead of one to obtain a modified visco-hyperelastic constitutive model, which can describe the mechanical response of nitrate ester plasticized polyether (NEPE) propellant in low and high strain-rate range. When the model is used to describe the mechanical behaviors of materials at low, intermediate, and high strain rates, more viscoelasticity elements need to be embedded, and thus it is difficult to optimize the values of any resulting material parameters. Empirical models, such as Johnson-Cook model, have also been used to describe the mechanical responses of polymers at different strain rates because of their simplicity, even though they may lack the support of the physical mechanisms.[20] Based on the idea, Song *et al.* [21] combined a modified Maxwell element and a Mooney function to form a rate-independent base model. Each of these two components was then multiplied by a rate-sensitive term to develop a rate-dependent model. Mohotti *et al.*[22] proposed a rate-dependent hyperelastic constitutive model with the assumption that strain energy potential is linearly dependent on the logarithm of strain rate. These empirical models, although simplistic, show good correlation with the experimental work, and are practical since they use few parameters.

The characterization of rate-dependent mechanical properties needs test data over a wide of strain rates as a physical basis. Numerous constant strain-rate tests have been carried out on the composite solid propellants. Experimental data corresponding to low strain rate ($\leq 10^{-1}$ s^{-1}),[23–25] and high strain rate (*c.* 10^{3} s^{-1})[26–28] were generally obtained using a universal testing machine, and an SHPB system, respectively. Intermediate strain rates (1 to 10^{2} s^{-1}) have received relatively little attention. Furthermore, HTPB propellant, under high overload conditions, deforms in such a strain-rate range. Therefore, reliable intermediate strain-rate experimental techniques need to be developed to obtain experimental data. Recently, a hydraulic testing machine has been used to investigate the mechanical properties of materials, such as steel,[29,30] polyuria,[22,31] and HTPB propellant,[32,33] at intermediate strain rates. In the present study, such a testing system is used.

In this work, a universal testing machine, a hydraulic testing machine, and an SHPB system are used to investigate the compressive mechanical properties of HTPB propellant at room temperature over strain rates ranging from 1.7×10^{-4} to 2500 s^{-1}. From experimental results, the rate-dependent characteristics are studied. Then a rate-dependent constitutive model is proposed to characterize the compressive mechanical properties of HTPB propellant at low, intermediate, and high strain rates.

EXPERIMENTAL

Material and Specimens

Table I lists the composition of the HTPB propellant investigated. For low strain rate compression testing, the specimens were designed as cylinders, with a diameter of 16 mm and a length of 20 mm. For intermediate strain rate compression testing, the specimens with dimensions identical to those used for the low strain rate compression testing were tested to eliminate any variability in the data caused by the choice of dimensions. For high strain rate compression testing, the specimens were cylindrical, with a diameter of 10 mm and a length of 5 mm. The length-to-diameter ratio of 1:2 and this relatively short length are necessary to minimize wave attenuation in the strain signals recorded,[34,35] and the effects of radial and longitudinal inertia in the specimen.[36] All specimens were machined from the same manufacturing batch, and stored in a desiccator cabinet before testing to eliminate any variability of compressive properties caused by humidity.

Low Strain Rate Compression Testing

Low strain rate compression testing of the HTPB propellant was performed as outlined in Table II. Each test was repeated at least five times. The force data from a load cell and the

Table II. Experimental Conditions from Low to Intermediate Strain Rate Compression Testing

Testing type	Low strain rate compression	Intermediate strain rate compression
Testing machine	Universal testing machine	Hydraulic testing machine
Average loading speed	0.2, 2, 20, 200 (mm/min)	20, 200, 700, 2200 (mm/s)
Engineering strain rate (1/s)	1.7×10^{-4}, 1.7×10^{-3}, 1.7×10^{-2}, 1.7×10^{-1}	1, 10, 35, 110
Temperature (°C)	Room temperature (20)	

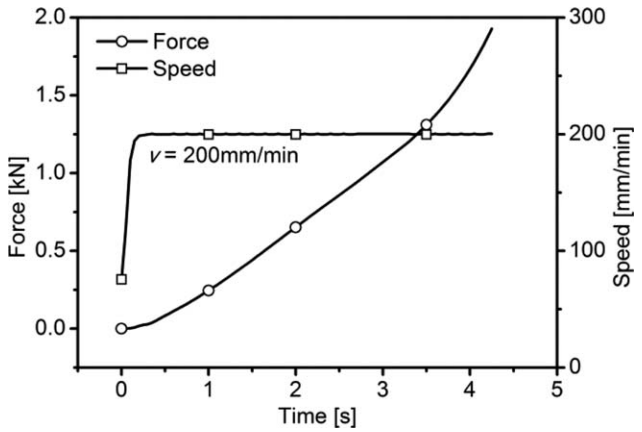

Figure 1. Typical loading case from low strain rate compression testing.

deformation data from an extensometer were recorded using data acquisition software. The corresponding engineering stress–engineering strain curves were calculated, and then plotted. A typical loading case from low strain rate compression testing is illustrated in Figure 1. Force increases under a constant loading speed, indicating that the specimen deforms at a constant engineering strain rate.

Intermediate Strain Rate Compression Testing

Intermediate strain rate compression testing of the HTPB propellant was performed as outlined in Table II, and the corresponding test requirements were the same as those used for the low strain rate compression testing. HTPB propellant is a highly energetic material. The energy of high-speed impact during loading may localize within a certain region in the specimen, resulting in the formation of "hot spots".[37,38] When the temperature in such "hot spots" is raised above that required for ignition, the specimen is ignited, and thus a large amount of hot gases is produced, constituting a potentially lethal occupational health and safety hazard. In this investigation, a protective setup was designed to protect testers from such danger. Figure 2(a,b) show the physical setup and schematic of the specimen loading without any protective setup, respectively; Figure 2(c,d) show the physical setup and schematic of the specimen loading with the protective setup, respectively. When the specimen burns under impact, the protective setup can prevent the diffusion of flame towards hydraulic oil covering the testing machine, and ensure that hot gases are delivered through the space between the baffle and protective wall. During the test, the specimen was located between the dynamic, and static, anvils. The dynamic anvil was driven, by a hydraulic piston, into the specimen at a pre-set speed over a pre-set distance. The reserved clearance ensured that the dynamic anvil has reached its target speed before imparting a strain to the specimen.

To ensure valid testing conditions, it is necessary to check whether, or not, the engineering strain rate during loading is constant, and if the protective setup induces any variability in the recorded compressive curves. Figure 3 shows typical loading cases from intermediate strain rate compression testing. From Figure 3(a,b), force increases under a nearly constant loading speed, indicating that, for testing at 1 and 10 s^{-1}, the engineering strain rate during loading is constant within phase "AC". From Figure 3(c,d), the loading speed decreases when force increases, indicating that, for testing at 35 and 110 s^{-1}, the engineering strain rate during loading gradually decreases within phase "AC". To obtain stress–strain curves at a constant engineering strain rate, only the data corresponding to phase "AB" is considered in the following analysis. The engineering strain rate is regarded as a constant case because of the small difference between the two loading speeds corresponding to points "A" and "B"; it is calculated from the average speed within phase "AB". Figure 4 shows a comparison between the curves obtained on a hydraulic testing machine with, and without, the protective setup. The two curves show good agreement, indicating that the effect of the protective setup on the testing curves

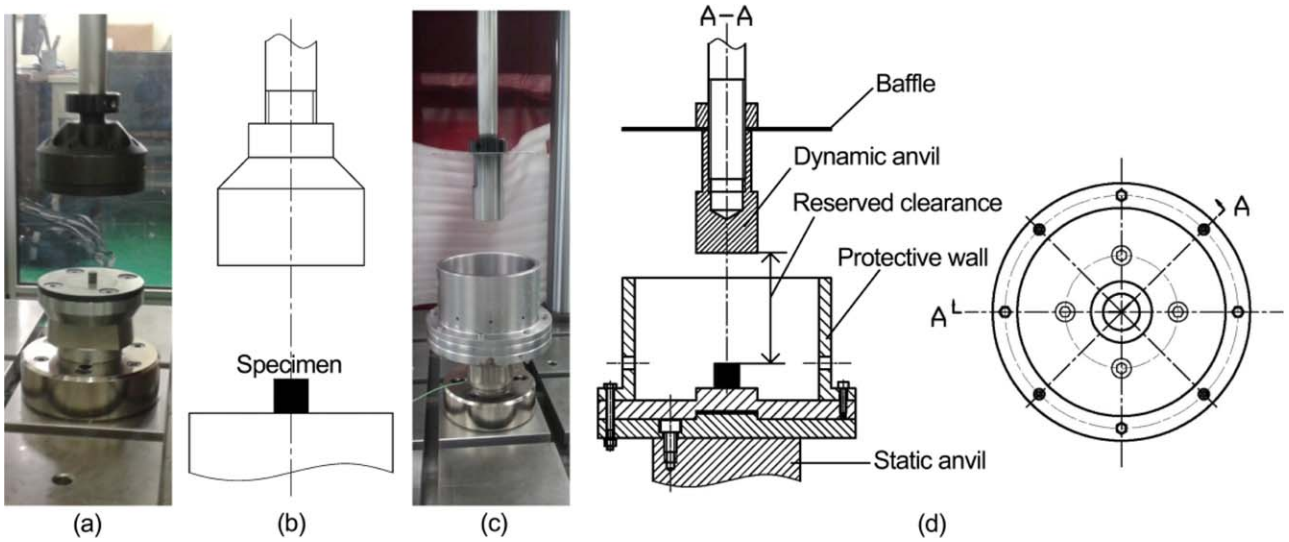

Figure 2. Physical setup and schematic of specimen loading. (a) and (b) without protective setup, (c) and (d) with protective setup. [Color figure can be viewed in the online issue, which is available at wileyonlinelibrary.com.]

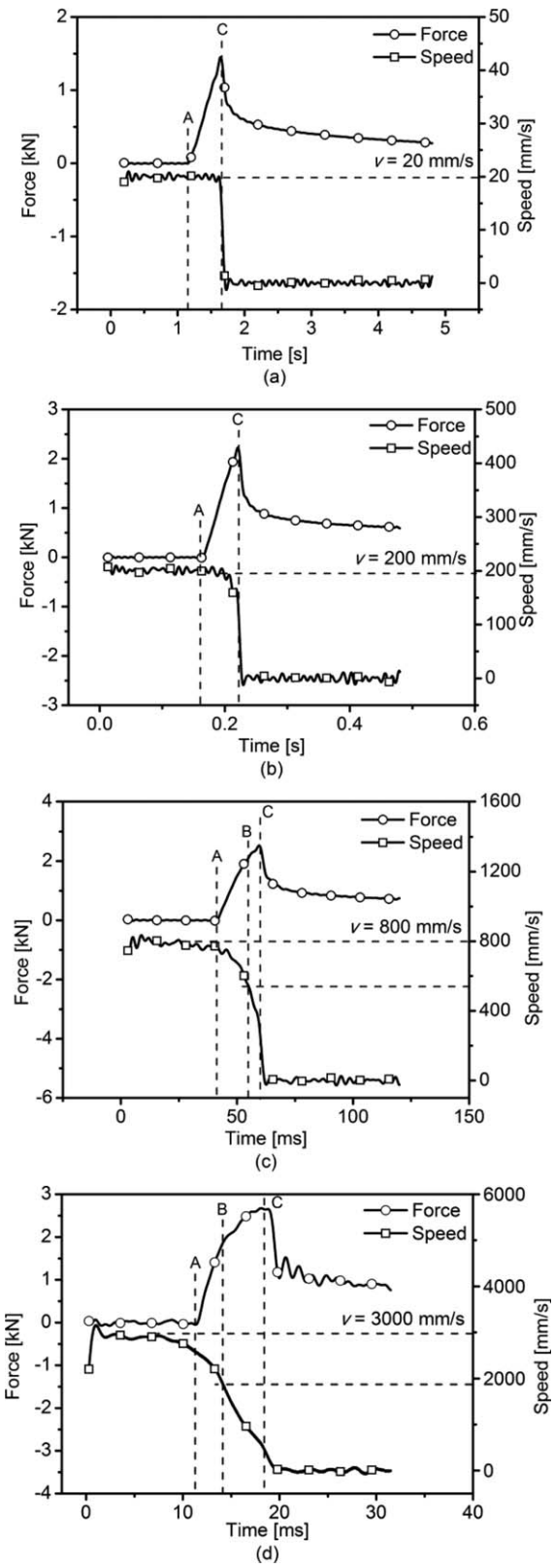

Figure 3. Typical loading cases from intermediate strain rate compression testing. (a) 1 s^{-1}, (b) 10 s^{-1}, (c) 35 s^{-1}, (d) 110 s^{-1}. "A" is the starting point for any loading, "B" is a point at which the loading speed is 70% of that at point "A", "C" is the end point for any loading.

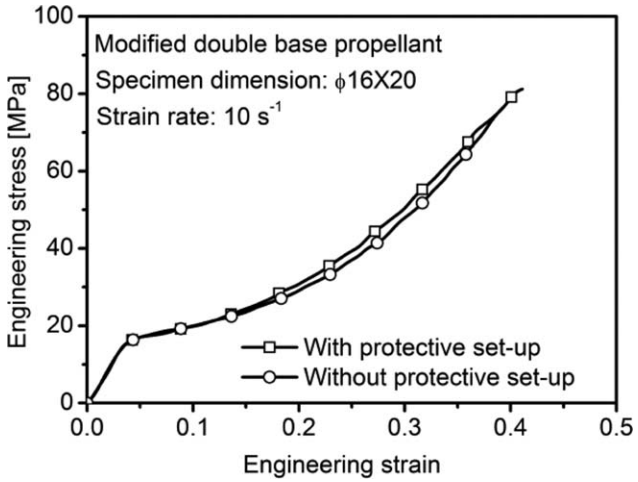

Figure 4. Comparison between the curves obtained on a hydraulic testing machine with, and without, the protective setup.

may be ignored. Therefore, it is concluded that intermediate strain rate compression testing was performed under valid testing conditions.

High Strain Rate Compression Testing

High strain rate compression testing of the HTPB propellant was performed as outlined in Table III. Each test was repeated at least five times. Figure 5 shows a schematic of the SHPB setup used here. The geometry and material properties of the bars are summarized in Table IV, in which m, D, L, and C were experimentally measured, ρ was calculated from m, D, and L, and E was calculated from ρ and C. During testing, the specimen was sandwiched between the incident bar and the transmission bar. The gas gun fired the striker bar to impact the incident bar, thus generating an incident strain pulse. When the pulse travelled to the interface between the incident bar and the specimen, a portion was reflected into the incident bar, and the remaining portion was transmitted into the transmission bar. The incident, reflected, and transmitted strain pulses were recorded from strain gauges mounted on the bars, and scanned at a sampling rate of 10 MHz and at 500 × magnification. The corresponding engineering stress-engineering strain curves were calculated, and then plotted. A protective box was used to protect testers against the danger from the possible burning of the specimen caused by high-speed impact. To obtain valid testing data on the low-impedance HTPB propellant, the SHPB setup used here, compared to the conventional setup, had three modifications: copper disks as pulse shapers were used to ensure a

Table III. Experimental Conditions from High Strain Rate Compression Testing

Machine	Gauge pressure (MPa)	Engineering strain rate (1/s)	Temperature (°C)
SHPB	0.015, 0.03, 0.08	700, 1400, 2500	Room temperature (20)

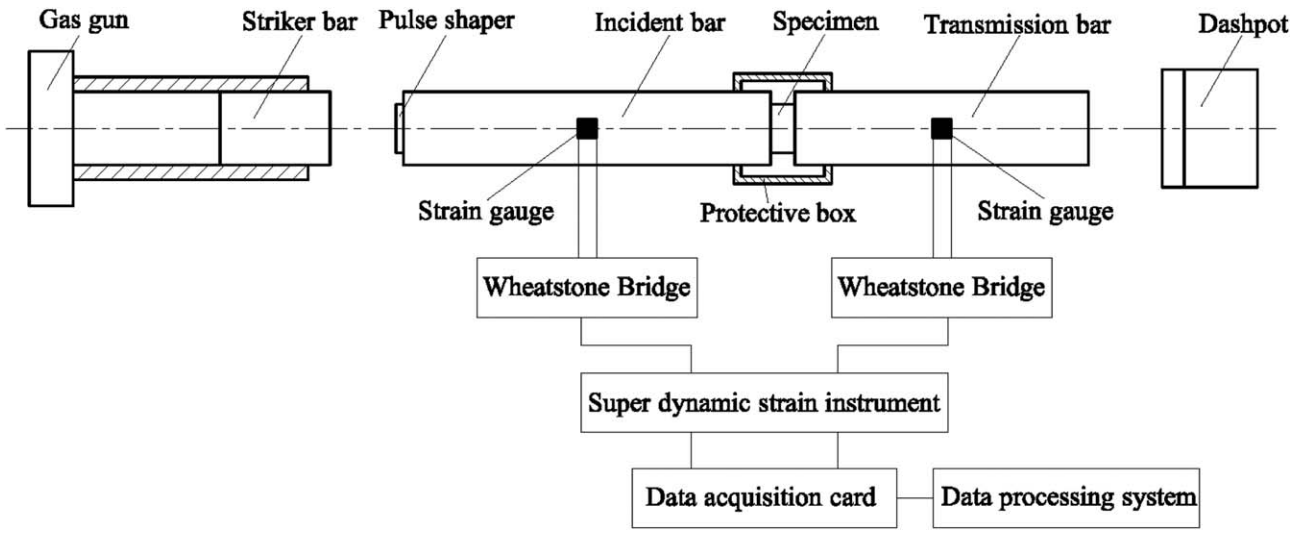

Figure 5. Schematic of the SHPB setup.

constant strain rate and dynamic stress equilibrium in the specimen by controlling the profile of the incident pulse[39]; the method saw a high-strength aluminum alloy used as the bar material rather than steel, and the transmission bar was hollow, which increased the amplitude of transmitted strain pulse[35]; petroleum jelly was used to lubricate the interfaces between the bars and the specimen to reduce friction.

Figure 6 demonstrates a typical set of incident, reflected, and transmitted signals from SHPB experiment on HTPB propellant at a strain rate of 700 s^{-1}. As shown in Figure 6, high-frequency components caused by high-speed impact towards the incident bar are not embodied in the incident signal. This is the result filtered out by the pulse shaper, and it is necessary to eliminate experimental error caused by dispersion in high-frequency components. The plateau-like region in the reflected signal indicates that the specimen deforms at a constant engineering strain rate. A common approach to check dynamic stress equilibrium in the specimen is to compare the axial force at its front end (facing the incident bar), F_1, to that at its back end (facing the transmission bar), F_2. The values of F_1 and F_2 are calculated from eqs. (1a) and (1b), respectively, based on one-dimensional stress wave theory.[40]

$$F_1 = F_I + F_R = A_I E_I \varepsilon_I(t) + A_I E_I \varepsilon_R(t) \quad (1a) \qquad F_2 = F_T = A_T E_T \varepsilon_T(t) \quad (1b)$$

where $\varepsilon_I(t)$, $\varepsilon_R(t)$, and $\varepsilon_T(t)$ are the incident, reflected, and transmitted strain pulses, respectively; F_I, F_R, and F_T are calculated from the incident, reflected, and transmitted strain pulses, respectively; A_I and E_I are the cross-sectional area and Young's modulus of the incident bar, respectively; A_T and E_T are the cross-sectional area and Young's modulus of the transmission bar, respectively. However, this procedure contains significant error for the low-impedance HTPB propellant because of the similar amplitude of the incident and reflected strain pulses (see Figure 6). In the present work, the dynamic stress equilibrium of the specimen was checked by comparing F_R to the difference between F_T and F_I, as shown in Figure 7. Two force histories corresponding to F_R and the difference between F_T and F_I nearly overlap, indicating that the specimen deforms under dynamic stress equilibrium. During the test, the specimen deformed at a constant engineering strain rate under dynamic stress equilibrium, indicating that high strain rate compression testing was performed under valid testing conditions.

RESULTS AND DISCUSSION

The compressive results of HTPB propellant across all tested strain rates are summarized in Figure 8, where the curves presented are averages of the repeatable results measured under each testing condition. Concerning the stress–strain curves, the maximum value of the engineering strain is set to 50%. This is based on the consideration that the solid propellant grain in the high overload applications generally deforms within the strain level of 50%. In the case of SHPB testing, the maximum value of the engineering strain in the specimen is dominated by the length and velocity of striker bar, and the intrinsic properties of the material, which is quite different from the experimental principles in the low, and intermediate strain rate compression

Table IV. Parameters of the Bars Used in the SHPB Setup

Bar type	Mass m (g)	Diameter D (mm)	Length L (mm)	Density ρ (kg/m^3)	Wave speed C (m/s)	Young's modulus $E = \rho C^2$ (GPa)
Striker bar	—	19.1	450	-	-	-
Incident bar	1163.2	19.1	1499	2680	5024	68.38
Transmission bar	264.8	Outer diameter: 16.4 Inner diameter: 12.6	1200	2550	5015	64.13

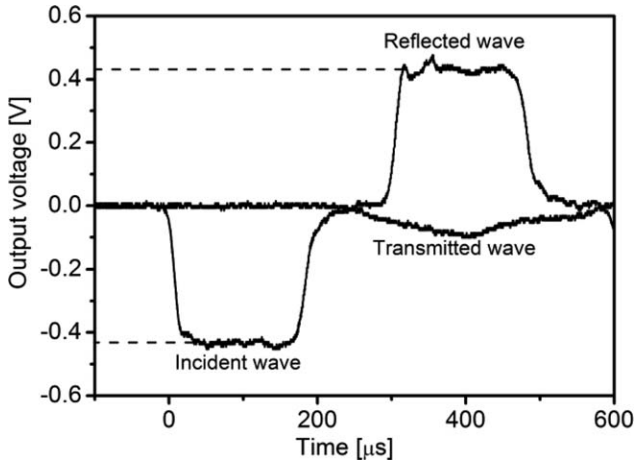

Figure 6. Typical set of incident, reflected, and transmitted signals.

testing. The higher strain rate corresponds to the higher loading amplitude and energy input, which results in a larger final strain in the specimen. Thus, the final strain of all stress–strain curves during the high strain rate loading is not equal to 50%, and increases with an increase in the strain rate. The increase of the final strain with the strain rate can also be observed in the published literatures related to the SHPB testing.[7–9,41] For all tested stress–strain curves, the stress increases in a quasi-linear manner when the strain becomes large. Furthermore, the mechanical properties of HTPB propellant are strongly dependent on the strain rate. In particular, the stress at a given strain increases with increasing strain rate. These mechanical characteristics will have to be taken into account in the development of constitutive model capable of predicting the mechanical response of HTPB propellant over a wide range of strain rates. In what follows, we will carefully study the influence of the strain rate on the mechanical response of HTPB propellant.

Figure 9 shows the engineering stress of HTPB propellant as a function of the logarithm of strain rate at different strains: 0.1, 0.2, 0.3, 0.4, and 0.5. The data points are directly obtained from the engineering stress–engineering strain curves at various strain rates (see Figure 8). The solid and dashed lines are, respectively,

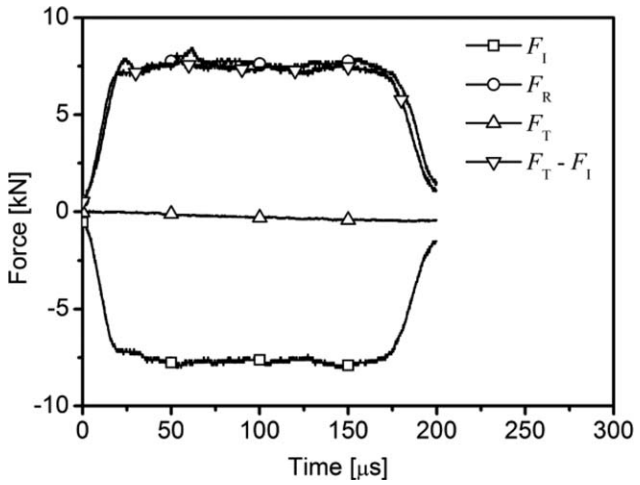

Figure 7. Force histories calculated from different signals.

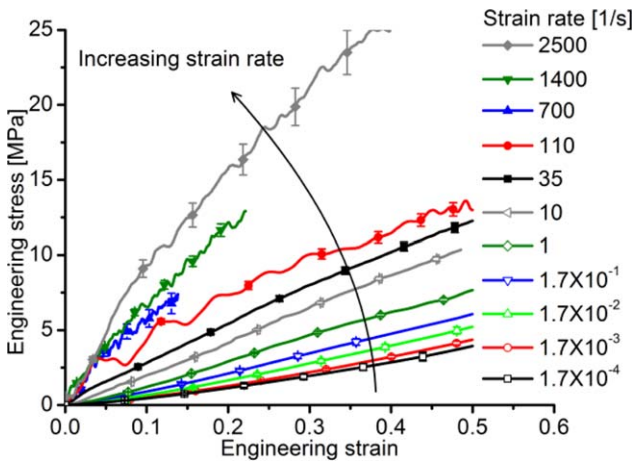

Figure 8. Compressive curves of HTPB propellant across all tested strain rates. The error bars represent the standard deviation. [Color figure can be viewed in the online issue, which is available at wileyonlinelibrary.com.]

generated from the linear and exponential fitting of the data points, and their specific expressions are listed in Table V. For all strain levels, the engineering stress increases linearly with the logarithm of strain rate when the strain rate is lower than 1 s^{-1}, and increases in an exponential manner with the logarithm of strain rate when the strain rate is higher than 1 s^{-1}. It is clear that HTPB propellant begins to undergo a significant material transition as the strain rate is increased beyond 1 s^{-1}. The mechanical properties in this HTPB propellant, before and after the transition, are dominated by different rate-dependent mechanisms.

The rate-dependent behavior shown in Figure 9 can be explained in terms of molecular-level motions. HTPB propellant is a particle-filled polymer. Its motion unit can be described on a variety of different length scales. The time taken by the motion of each unit, called the relaxation time, increases with

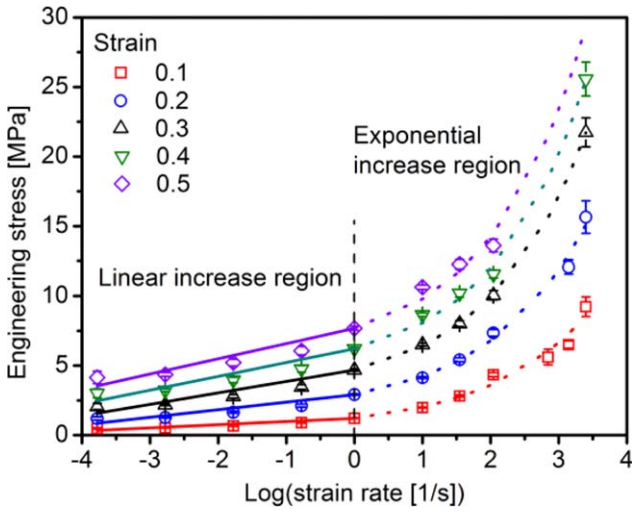

Figure 9. Engineering stress as a function of the logarithm of strain rate at different strains. [Color figure can be viewed in the online issue, which is available at wileyonlinelibrary.com.]

Table V. Specific Expressions of Fitted Functions Shown in Figure 9

Fitted function		Linear increase region $\sigma=A_1+A_2\log\dot{\varepsilon}$		Exponential increase region $\sigma=B_1+B_2\exp(B_3\log\dot{\varepsilon})$		
		A_1	A_2	B_1	B_2	B_3
Strain	0.1	1.22	0.23	0.38	0.84	0.67
	0.2	2.92	0.54	1.61	1.31	0.69
	0.3	4.69	0.82	3.05	1.64	0.72
	0.4	6.22	0.99	4.54	1.68	0.74
	0.5	7.68	1.10	5.74	1.94	0.73

its length. Thus, the motion of unit with a larger length scale will be firstly restricted with an increase in strain rate. The restriction of molecular mobility at a certain strain rate will make the molecular chains stiffer, which contributes to the resistance between adjacent molecular segments, and the strengthened resistance would cause the initial modulus and stress to increase significantly. The mechanical behavior of HTPB propellant is similar to that of a variety of polymers studied by many researchers.[6–9] In their studies, the bilinear dependence of the stress at a given strain, or the yield stress on the logarithm of strain rate was observed instead of the linear dependence, followed by the exponential dependence, because of a lack of experimental data at the intermediate strain rates. To study this bilinear behavior, DMA testing was performed. The storage modulus, loss modulus, and loss tangent were measured as a function of temperature at various frequencies. By approximating the applied sinusoidal strain wave with a triangular strain wave in DMA testing, the frequency dependence was expressed as an equivalent strain-rate dependence: this is computed from the test frequency and preset loading amplitude. It was found that the transition location of the storage modulus shifts to a higher temperature in a linear manner with the equivalent strain rate. When the transition location shifts past room temperature, the materials studied will be transformed from a state to another. Because of the difference in the rate-dependent mechanism between two material states, the mechanical properties of these materials at room temperature are bilinearly dependent on the logarithm of strain rate. The glass transition plays a role in bilinear behavior when the material is in a rubbery state at room temperature, and the low order transition plays a role in bilinear behavior when the material is in a glassy state at room temperature.

CONSTITUTIVE MODEL

An empirical model to characterize the rate-dependent behavior of HTPB propellant typically takes the form

$$\sigma=f(\varepsilon,\dot{\varepsilon}_0)g(\dot{\varepsilon}/\dot{\varepsilon}_0) \tag{2}$$

where σ and ε are stress and strain, respectively; $f(\varepsilon,\dot{\varepsilon}_0)$ represents the rate-independent behavior at the reference strain rate $\dot{\varepsilon}_0$; $g(\dot{\varepsilon}/\dot{\varepsilon}_0)$ accounts for the effects of strain rate.

Table VI. Values of the Parameters

E (MPa)	A	B_1	B_2
15.22	0.1614	0.6753	0.7516

Because of the close-linear dependence of the stress of HTPB propellant on the strain for all tested strain rates, $f(\varepsilon,\dot{\varepsilon}_0)$ is assumed to be

$$f(\varepsilon,\dot{\varepsilon}_0)=E\varepsilon \tag{3}$$

where E is a material parameter, and can be considered as an equivalent modulus of HTPB propellant at the reference strain rate $\dot{\varepsilon}_0$.

By combining $g(\dot{\varepsilon}_0/\dot{\varepsilon}_0)=1$ and the rate-dependent mechanical properties of HTPB propellant shown in Figure 9, $g(\dot{\varepsilon}/\dot{\varepsilon}_0)$ can be expressed by

$$g(\dot{\varepsilon}/\dot{\varepsilon}_0)=\begin{cases}1+A\log(\dot{\varepsilon}/\dot{\varepsilon}_0) & \dot{\varepsilon}\le 1\mathrm{s}^{-1}\\ B_1+(1-B_1)\exp[B_2\log(\dot{\varepsilon}/\dot{\varepsilon}_0)] & \dot{\varepsilon}>1\mathrm{s}^{-1}\end{cases} \tag{4}$$

where A, B_1, and B_2 are material parameters.

The resulting rate-dependent constitutive model, found by combining eqs. (2–4), is

$$\sigma=\begin{cases}E\varepsilon[1+A\log(\dot{\varepsilon}/\dot{\varepsilon}_0)] & \dot{\varepsilon}\le 1\mathrm{s}^{-1}\\ E\varepsilon\{B_1+(1-B_1)\exp[B_2\log(\dot{\varepsilon}/\dot{\varepsilon}_0)]\} & \dot{\varepsilon}>1\mathrm{s}^{-1}\end{cases} \tag{5}$$

The parameters in this model are fitted by least squares approach; the specific procedures are as follows:

1. Taking 1 s^{-1} as the reference strain rate and the corresponding stress as the reference stress, the parameter E in eq. (3) is fitted by the reference curve, and the resulting value is listed in Table VI.

2. The term $g(\dot{\varepsilon}/\dot{\varepsilon}_0)$ is fitted by the curves at various strain rates. The resulting values are plotted as a function of the logarithm of relative strain rate, as shown in Figure 10. It can be

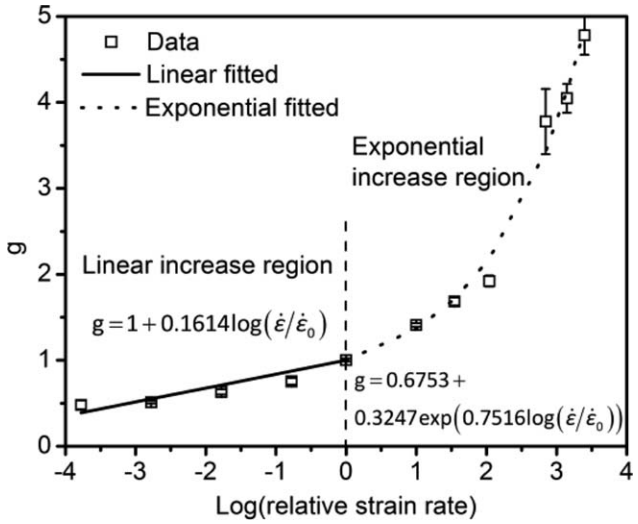

Figure 10. Function g as a function of the logarithm of relative strain rate.

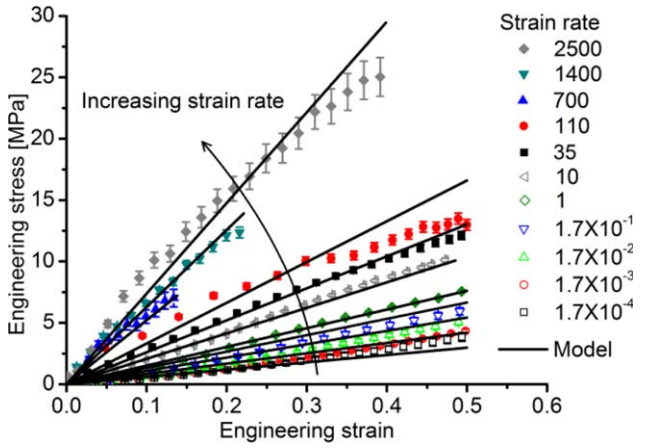

Figure 11. Comparison of model and experimental data. [Color figure can be viewed in the online issue, which is available at wileyonlinelibrary.com.]

seen that the term $g(\dot{\varepsilon}/\dot{\varepsilon}_0)$ increases linearly with the logarithm of relative strain rate when the strain rate is lower than 1 s^{-1}, and increases in an exponential manner with the logarithm of relative strain rate when the strain rate is higher than 1 s^{-1}. This change in trend of the $g(\dot{\varepsilon}/\dot{\varepsilon}_0)$ with the logarithm of relative strain rate again confirms the rate-dependent mechanical behavior of HTPB propellant shown in Figure 9. Values of parameters A, B_1, and B_2 are listed in Table VI.

Figure 11 demonstrates a satisfactory correlation between the model curves and the experimental data under most experimental conditions, indicating the potential of the rate-dependent constitutive model proposed to describe the compressive mechanical properties of HTPB propellant over a wide range of strain rates. However, there is a bigger deviation between the model and the experimental data at the strain rates of 110 and 2500 s^{-1}. The empirical model for this HTPB propellant is proposed with the assumption that the stress linearly increases with strain at all tested strain rates. The linearity in the assumption is unsuitable for the prediction of the nonlinear mechanical behaviors at higher strain rates and at larger strain. This may be why there is such a deviation between the model curves and experimental data under the two tested strain rates. A modification of the empirical model will be proposed for the description of the nonlinear response in the future work.

CONCLUSIONS

This research is the first to conduct compression testing of HTPB propellant at low, intermediate, and high strain rates (1.7×10^{-4} to 2500 s^{-1}). Results show that the increasing trend in stress at a given strain with the logarithm of strain rate changes from a linear to an exponential form at 1 s^{-1}. The rate dependence of HTPB propellant is attributed to the restriction of molecular mobility with a certain length scale.

By combining the linear dependence of stress on strain and the change in trend of stress with the logarithm of strain rate in HTPB propellant, a rate-dependent constitutive model is proposed. The model comprises a linearly elastic component and a rate-dependent component. The linearly elastic component is considered as a base model from which the characterization of the linearly elastic behavior of HTPB propellant at the reference strain rate may be undertaken. The rate-dependent component is then multiplied into the linearly elastic component to describe the strain-rate dependence.

The proposed model can describe the compressive mechanical properties of HTPB propellant at strain rates from 1.7×10^{-4} to 2500 s^{-1}. The model has relatively a small number of material parameters and a simple form of expression, increasing its applicability in numerical simulations.

ACKNOWLEDGMENTS

This work was funded by the National Natural Science Foundation of China (Grant No. 11402025).

REFERENCES

1. Kakavas, P. A. *Int. J. Solids Struct.* **2014**, *51*, 2019.
2. Zalewski, R.; Wolszakiewicz, T. *Cent. Eur. J. Energ. Mater.* **2011**, *8*, 223.
3. Sui, X.; Wang, N.; Wan, Q.; Bi, S. *Propellants Explos. Pyrotech.* **2010**, *35*, 535.
4. Deng, B.; Xie, Y.; Tang, G. *Propellants Explos. Pyrotech.* **2014**, *39*, 117.
5. Chou, S. C.; Robertson, K. D.; Rainey, J. H. *Exp. Mech.* **1973**, *13*, 422.
6. Siviour, C. R.; Walley, S. M.; Proud, W. G.; Field, J. E. *Polymer* **2005**, *46*, 12546.
7. Mulliken, A. D.; Boyce, M. C. *Int. J. Solids Struct.* **2006**, *43*, 1331.
8. Jordan, J. L.; Foley, J. R.; Siviour, C. R. *Mech. Time-Depend. Mater.* **2008**, *12*, 249.
9. Yi, J.; Boyce, M. C.; Lee, G. F.; Balizer, E. *Polymer* **2006**, *47*, 319.
10. Walley, S. M.; Field, J. E.; Pope, P. H.; Safford, N. A. *Philos. Trans. R. Soc. Lond. A* **1989**, *328*, 1.
11. Walley, S. M.; Field, J. E.; Pope, P. H.; Safford, N. A. *J. Phys. III* **1991**, *1*, 889.
12. Walley, S. M.; Field, J. E. *Dymat J.* **1994**, *1*, 211.
13. Bergström, J. S.; Boyce, M. C. *J. Mech. Phys. Solids* **1998**, *46*, 931.
14. Bergström, J. S.; Boyce, M. C. *Mech. Mater.* **2001**, *33*, 523.
15. Yang, L.; Shim, V. P. W.; Lim, C. T. *Int. J. Impact Eng.* **2000**, *24*, 545.
16. Shim, V. P. W.; Yang, L.; Lim, C. T.; Law, P. H. *J. Appl. Polym. Sci.* **2004**, *92*, 523.
17. Pouriayevali, H.; Guo, Y.; Shim, V. P. W. *Int. J. Impact Eng.* **2012**, *47*, 71.
18. Khajehsaeid, H.; Arghavani, J.; Naghdabadi, R.; Sohrabpour, S. *Int. J. Eng. Sci.* **2014**, *79*, 44.
19. Zhang, J.; Zheng, J.; Chen, X.; Sun, C.; Xu, J. *J. Eng. Mater. Technol.* **2014**, *136*, 337.

20. Chen, W.; Zhou, B. *Mech. Time-Depend. Mater.* **1998**, *2*, 103.
21. Song, B.; Chen, W.; Cheng, M. *J. Appl. Polym. Sci.* **2004**, *92*, 1553.
22. Mohotti, D.; Ali, M.; Ngo, T.; Lu, J.; Mendis, P. *Mater. Des.* **2014**, *53*, 830.
23. Duncan, E. J. S.; Margetson, J. *Propellants Explos. Pyrotech.* **1998**, *23*, 94.
24. Swanson, S. R.; Christensen, L. W. *J. Spacecraft* **1983**, *20*, 559.
25. Xu, J.; Chen, X.; Wang, H.; Zheng, J.; Zhou, C. *Int. J. Solids Struct.* **2014**, *51*, 3209.
26. Ho, S. Y. *J. Propul. Power* **2002**, *18*, 1106.
27. Siviour, C. R.; Laity, P. R.; Proud, W. G.; Field, J. E.; Porter, D.; Church, P. D.; Gould, P.; Huntingdon-Thresher, W. *Proc. R. Soc. Lond. A* **2008**, *464*, 1229.
28. Sun, C.; Xu, J.; Chen, X.; Zheng, J.; Zheng, Y.; Wang, W. *Mech. Mater.* **2015**, *89*, 35.
29. Xu, S.; Ruan, D.; Beynon, J. H.; Rong, Y. *Mater. Sci. Eng. A* **2013**, *573*, 132.
30. Paul, S. K.; Raj, A.; Biswas, P.; Manikandan, G.; Verma, R. K. *Mater. Des.* **2014**, *57*, 211.
31. Raman, S. N.; Ngo, T.; Lu, J.; Mendis, P. *Mater. Des.* **2013**, *50*, 124.
32. Wang, Z.; Qiang, H.; Wang, G.; Huang, Q. *J. Appl. Polym. Sci.* **2015**, *132*, 42104.
33. Wang, Z.; Qiang, H.; Wang, G. *Propellants Explos. Pyrotech.* **2015**,
34. Gray, I. I. I.; Blumenthal, G.; Trujillo, W.; Carpenter, C.; Zh, R. *J. Phys. IV* **1997**, *7*, 523.
35. Chen, W.; Zhang, B.; Forrestal, M. *J. Exp. Mech.* **1999**, *39*, 81.
36. Davies, E. D. H.; Hunter, S. C. *J. Mech. Phys. Solids* **1963**, *11*, 155.
37. Taylor, W.; Weale, A. *Proc. R. Soc. Lond. A* **1932**, *138*, 92.
38. Taylor, W.; Weale, A. *Trans. Faraday Soc.* **1938**, *34*, 995.
39. Song, B.; Chen, W. *Exp. Mech.* **2004**, *44*, 300.
40. Kolsky, H. *Proc. Phys. Soc. Lond.* **1949**, *62*, 676.
41. Yu, P.; Yao, X.; Han, Q.; Zang, S.; Gu, Y. *Polymer* **2014**, *55*, 6577.